Lithuanian Journal of Physics, Vol. **55**, No. 4, pp. 297–304 (2015)

THE EFFECT OF LOW TEMPERATURE COATING AND ANNEALING ON STRUCTURAL AND OPTICAL PROPERTIES OF CdSe/CdS CORE/SHELL QDs

M. Isarov, N. Grumbach, G.I. Maikov, J. Tilchin, Y. Jang, A. Sashchiuk, and E. Lifshitz

Solid State Institute, Russell Berrie Nanotechnology Institute, Nancy and Stephen Grand Technion Energy Program, Schulich Faculty of Chemistry, Technion, 3200003 Haifa, Israel

E-mail: chaldona@tx.technion.ac.il; ssefrat@tx.technion.ac.il

Received 31 August 2015; accepted 29 September 2015

This paper presents the optical temperature dependent properties, over a wide range of temperatures from 4 to 300 K, of new CdSe/CdS core/shell colloidal quantum dots (QDs) with varying shell thickness coated and annealed at low temperature. It was demonstrated that low temperature coating and annealing processes enhanced the photoluminescence (PL) quantum yield accompanied by variation in the QDs structure, formation of an alloyed interface layer, suppression of the number of defects at the CdSe/CdS interface, band gap energy red-shift, narrowing of CdS longitudinal optical phonon band, and decrease of the PL inhomogeneous broadening parameter.

Keywords: CdSe/CdS core/shell structures, colloidal quantum dots, excitons, photoluminescence

PACS: 73.21.La, 72.22.-f, 73.61.Ga, 73.90.tf

1. Introduction

Colloidal quantum dots (QDs) are of considerable interest due to their size-dependent optical and electronic properties, which allow implementation in photovoltaic cells [1], light-emitting diodes [2], photocatalysis [3], bioassays [4], and electronics [5]. However, the photostability and emission efficiency of QDs show a strong dependence on surface quality [6]. This issue was dealt with by overcoating the QDs with an inorganic broad band gap material, forming a core/shell QDs structure [7–12]. These QDs show a significant improvement of the photoluminescence quantum yield (PL QY), as well as an increase in their photostability [13]. CdSe QDs are probably the most extensively investigated QDs, due to the simplicity of their preparation using hot-injection processes [14], enabling accurate control of particle size, shape, and size distribution [15, 16]. In the past decade, a new generation of high-quality CdSe/CdS QDs was produced at 310 °C, showing high PL QY and photostability [17, 18]. Another approach suggested the design of alloy composition at the core/shell interface to reduce the crystallographic mismatch and consequently lower the amount of defect sites [19, 20]. Such an alloyed interface also induces changes in carrier distribution with the existence of a graded interface potential [21], which led to a suppression of the Auger process in nanostructures [22–24]. In the latest work, a new concept of the thermal cycling procedure of shell deposition at low temperatures (140 °C) was applied to achieve high PL QY values up to 85% and sharp emission line widths [25]. Recently, in our group, a new comprehensive method [26], using low temperature coating at 100 °C with additional higher temperature annealing at 130 °C, was developed. Simple low temperature coating approaches allow controlling the formation of CdSe/CdS QDs with different shell thickness. A controlled post-coating annealing at elevated temperatures forms a thin alloy interface, achieving exceptionally

high quality materials, as pronounced in their high PL QY and stability. However, for applications in optoelectronic devices, detailed knowledge of the optical properties of these new core/shell QDs is required to understand the effect of low temperature shell growth and annealing on the crystallographic and electronic structure of CdSe/CdS core/shell QDs. In this paper, we present comparative experimental studies concerning the influence of the shell morphology on the optical properties of CdSe/CdS QDs with 3 monolayer (ML) and 6ML shells, using structural methods, Raman and optical spectroscopy in the temperature range from 4 to 300 K. It has been shown that the influence of the coating and annealing processes induces different exciton behaviour for 3ML and 6ML core/shell QDs on their optical properties. The results obtained demonstrate that low temperature coating and annealing led to enhanced PL QY and could be accompanied by variation in the core/shell QDs structure, due to reduction of lattice strain, suppression of the number of defects at the CdSe core surface and at the CdSe/CdS interface. In addition, the annealing process led to PL QY enhancement due to the formation of an alloyed interface, an additional band gap energy (E_g) red-shift, narrowing of a CdS longitudinal optical (LO) phonon band, and additional reduction of the PL inhomogeneous broadening parameter Γ_{inh}, obtained at 4 K.

2. Experiment

The synthesis and characterization of CdSe/CdS core/shell QDs using low temperature coating at 100 °C, with additional higher temperature annealing at 130 °C, was described in Ref. [26]. The synthesis procedure included three steps: in the first step, CdSe cores were grown according to the method developed previously [8]. In the second and third steps, CdSe/CdS core/shell QDs were prepared using a CdS shell coating program as follows: (1) the CdSe cores were coated with the CdS shell at 100 °C for a duration of two hours; (2) the coated CdSe/CdS core/shell QD samples were annealed at 130 °C for 90 min, allowing formation of an alloyed core/shell interface without changing the QDs size. The amounts of the added S precursors have been calculated to reach the shell thickness desired, in general, 3ML and 6ML, where one ML corresponds to an increase of 0.33 nm of the QD radius (r). The QD samples obtained after the coating and annealing stages are referred to hereafter as samples before annealing (BA) and after annealing (AA).

Five QD samples including one CdSe core sample with radius of r = 1.7 ± 0.5 nm and four CdSe/CdS core/shell samples BA and AA with 3ML and 6ML, referred to as BA 3ML, BA 6ML, AA 3ML and AA 6ML, were then studied by crystallographic measurements, Raman, and optical spectroscopy in a temperature range from 4 to 300 K. For this study, the QDs were (1) dissolved in hexane; (2) drop-casted on a Si wafer; or (3) dispersed into an ultraviolet (UV) epoxy resin. The epoxy resin was prepared from commercially available epoxy resin (Super Sap CCR Epoxy) and slow hardener (Super Sap CCS), based on polyoxypropylenediamine (CAS# 9046-10-0). The epoxy resin did not affect the shape and energy position of absorption and PL spectra.

The samples' crystal structure was obtained using transmission electron microscopy (TEM) and X-ray powder diffraction (XRD) measurements. The QDs size and shell thicknesses were determined by a direct analysis of TEM images, which were recorded with a JEOL 2200 FS electron microscope. XRD patterns were obtained by a *Philips* PW1830 X-ray diffractometer. Raman spectra were performed using a micro-Raman spectrometer (*Horiba Jobin Yvon* XploRa) in which excitation was provided by an Nd:YAG laser at 532 nm. UV–VIS absorption spectra of the QDs were recorded using a *JASCO* V-570 UV–VIS–NIR spectrometer. PL measurements were performed on a homemade fluorescence system. PL QY was determined relatively to Rhodamine 6G dissolved in ethanol (PL QY of Rhodamine 6G in ethanol = 95%).

3. Results and discussion

Structural properties of CdSe and CdSe/ CdS QDs obtained at room temperature (RT) are summarized in Fig. 1. Figure 1(a) displays the TEM images of the CdSe core with a radius of 1.7 ± 0.5 nm, and Fig. 1(b) shows the corresponding core/shell QDs sample BA 3ML with r = 2.7 ± 0.5 nm, revealing the monodispersity of the spherically-shaped CdSe cores and core/shell QDs with slightly inhomogeneous, asymmetric shapes. TEM images of BA 6ML and AA 6ML core/shell QDs (not shown here) indicate that their radius is r = 3.7 ± 0.5 nm. Figure 1(c) displays the XRD patterns of the core CdSe QDs (red curve online, the lowest) and CdSe/CdS QDs (blue and green curves online, the middle and the highest ones), obtained after different stages of the coating/annealing processes (see legend). The vertical lines represent the XRD lines of bulk CdSe zinc blende (zb) (soft vertical lines), and CdS zb (bold vertical lines), indicated in the legend. The XRD spectrum of CdSe/CdS core/shell samples BA 3ML shows a shift toward larger 2θ values in respect to that of the CdSe core sample. A more pronounced shift was found in the XRD spectrum of the AA 3ML sample,

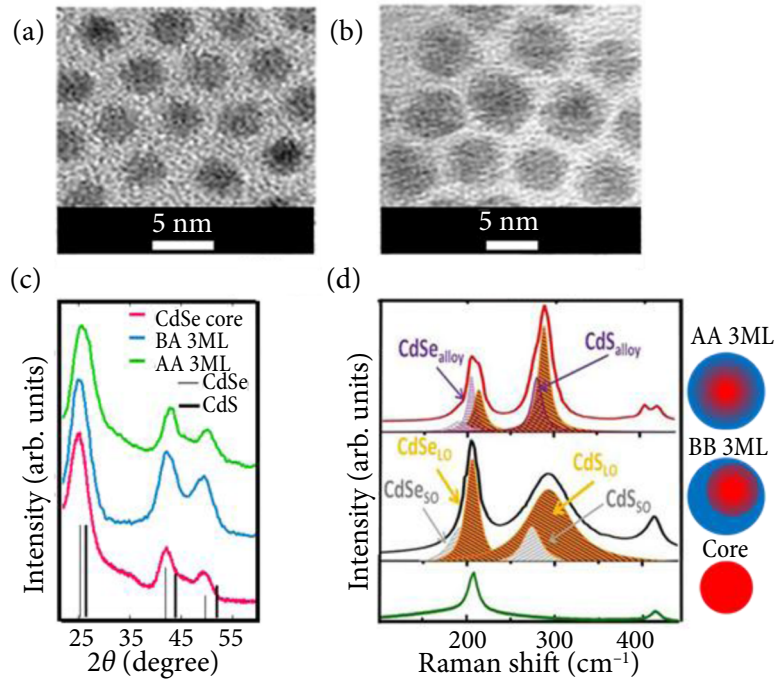

Fig. 1. TEM images of (a) CdSe core (r = 1.7 ± 0.5 nm) and (b) CdSe/CdS core/shell 3ML QDs sample before annealing (BA) with r = 2.7 ± 0.5 nm. (c) XRD patterns of CdSe core and CdSe/CdS core/shell QD samples as given in the legend. QDs indexed to the bulk zinc blende crystal structures of CdSe and CdS, as shown in the legend. (d) Raman spectra of CdSe core (green line online, the lowest), core/shell CdSe/CdS sample BA 3ML after coating at 100 °C (black line), and 3ML sample after annealing (AA) at 130 °C (red line online, the topmost). Schematic images of different 3ML core/shell structures are shown on the right. All measurements were performed at RT under air conditions.

annealed at 130 °C, supporting the occurrence of alloying at the core/shell interface during the annealing process. The XRD spectra of core/shell QDs are between those of zinc blende CdSe and CdS.

Crystallographic changes in the core or shell areas can be monitored by observing the evolution of the corresponding Raman signal. Figure 1(d) exhibits Raman spectra in the range of 100–450 cm^{-1}, performed on r = 1.7 ± 0.5 nm core CdSe QDs and on the corresponding CdSe/CdS QDs with a shell thickness of 3MLs, before and after the annealing processes (see legend). The Raman spectrum of core QDs shows a single dominant band at 206.8 cm^{-1} (25.5 meV), related to the fundamental LO phonon of CdSe. The spectrum of 3ML core/shell QDs after coating shows two asymmetric bands, corresponding to the LO phonon contribution of the core CdSe (near 206 cm^{-1}) and the shell CdS near 293 cm^{-1}, whereas each band consists of two sub-bands (see Lorentzian function fits), related to the first-order LO phonons and to surface optical (SO) phonons at 184 and 285 cm^{-1}. It should be noted that the width of the CdS LO band is broad (about 60 cm^{-1}) and might result from the phonon confinement as well as from the non-uniformity of shell thickness among the QD cores [27]. The shell thickness inhomogeneity signifies that the 3ML shell grown around the core is not concentric as shown schematically in Fig. 1(d). The Raman spectrum of these core/shell QDs after the annealing stage exhibits the appearance of additional sub-bands at 187 cm^{-1} and at overlapping the CdSe and the CdS spectral features at 289.2 cm^{-1} (see purple-coloured online Lorentzian functions), associated with the LO mode of the CdSe$_x$S$_{1-x}$ alloyed component [19, 21–24, 28], marked as CdSe$_{alloy}$ and CdS$_{alloy}$ in the figure. A significant narrowing of the CdS phonon LO band (25 cm^{-1}) reveals higher homogeneity of CdS shell thickness thus suggesting formation of a concentric core/shell structure, as presented schematically in Fig. 1(d). Furthermore, the intensity of CdS band is 1.5 times higher than that of CdS$_{alloy}$, revealing the existence of a thin interfacial alloyed layer. Thus, the Raman spectrum suggests that the coating stage at 100 °C (with the amount of added S precursor required to reach 3ML shell) produces CdSe/CdS QDs with inhomogeneous shell thickness, due to the lattice mismatch between the core and shell material causing lattice strain at the interface. In contrast, the low temperature (130 °C) annealing stage can induce inter-diffusion of the core and shell materials, creating an alloyed interfacial layer, reducing the lattice strain, and inducing the formation of a CdSe/CdS structure with homogenous (more symmetric) shell thickness, defined as a "concentric" structure.

Figure 2(a) displays the absorbance (dashed curves) and PL (solid curves) spectra of core CdSe QDs with an average r = 1.7 ± 0.5 nm (red online, the bottom) and of the corresponding CdSe/CdSQDs samples BA 3ML (blue online, second from the bottom), AA 3ML (green online, third from the bottom), BA 6ML (black online, fourth from the bottom), and AA 6ML (magenta online, fifth from the bottom), extracted during shell growth and annealing processes.

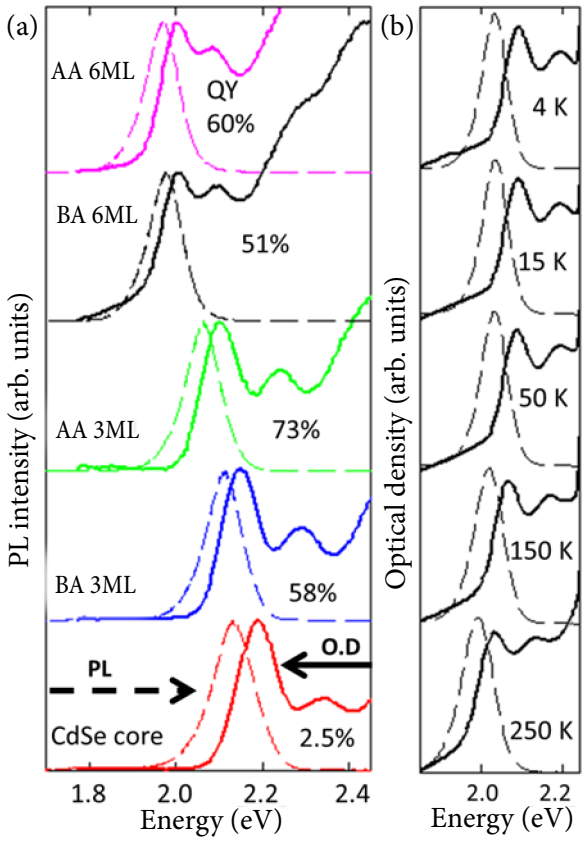

Fig. 2. (a) Normalized absorption (solid lines) and PL (dashed lines) spectra of the CdSe core with r = 1.7 nm and the corresponding CdSe/CdS QDs after coating at 100 °C with 3ML and 6ML, and after their annealing at 130 °C, as shown in the legend. The QDs were dissolved in hexane solution and recorded at RT. The PL QY of samples investigated is indicated on the right. (b) Representative temperature-dependent absorption and PL spectra of CdSe/CdS BA 6ML QDs dispersed in epoxy resin, the temperatures are given on the right.

The QD samples were dissolved in hexane and measured at RT. The spectra in Fig. 2(a) are dominated by the first excitonic transitions with energy $E_{1Sh3/2-1Se1/2}$, which are referred to as band-gap energy (E_g). The optical measurements show that the QDs obtained are high quality samples with well-defined excitonic transitions in the absorption spectra and narrow absorption and PL transitions bands. The plot presents a red-shift of E_g in the core/shell structure during shell growth with respect to the E_g of the CdSe cores, caused by the electron wave function extending into the CdS shell due to a low energy barrier between the conduction bands of CdSe and CdS semiconductors. The magnitude of the E_g red-shift, during the shell growth, as shown in Fig. 2(a), is greater for 6ML QDs (black lines) and is about 190 meV. This value is consistent with the data obtained in literature [7] for the same size CdSe/CdS QDs coated at high temperatures. In contrast, the observed E_g red-shift during the shell growth in the 3ML sample (40 meV) is less than that in the same size CdSe/CdS QDs coated at higher temperature, >140 °C [25]. This phenomenon can be explained by inhomogeneous (irregular) thickness shell growth at low T = 100 °C [27] and is supported by a broad CdS LO band in the Raman spectrum shown in Fig. 1(d). Further, as seen in Fig. 2(a), annealing of QDs with a 3ML shell causes an additional red-shift of E_g up to 50 meV, which can be attributed to inter-diffusion of the core and shell materials, creating an alloyed interfacial layer which reduces the lattice strain, and induces the formation of the CdSe/CdS structure with homogenous (more symmetric) shell thickness. This is supported by Raman CdS peak narrowing with the formation of a thin interfacial alloyed layer (Fig. 1(d)).

The red-shift (up to 26 meV) in the E_g on annealing at 210 °C of CdSe/CdS core/shell QDs, identical in size to our samples, was obtained and calculated recently by D. Kelley in Ref. [29]. The result was explained by the release of strain pressure on the core. It has also been recently shown [30] that the generation of concentric core/shell QDs could cause a red-shift (5–40 meV) of E_g. The experimental observation was supported by the calculation [30] based on the effective mass approximation, which predicted a red-shift of E_g as well as a possible reduction of the electron-hole overlap integral upon displacement of the core and shell centers with respect to each other. Annealing of QDs with a 6ML shell causes smaller E_g red-shifts (up 13 meV) in the absorption and emission spectra, explained by reduction in the lattice strain and is in the same value range [29]. The PL QY of the samples investigated are presented on the right side of Fig. 2(a), and show that QY increased from 2.5% for core samples to at least 58% for core/shell samples with 3ML shell thickness. This is the result of the reduction in the number of CdSe surface defects due to the coating of the core with an inorganic shell, which will be presented later in Fig. 3(c). The PL QY of the samples with BA 6ML is about 51%, this value is consistent with the data obtained for the same size core/shell QDs created at high temperature published in literature [25, 31].

An additional enhancement of the PL QY after annealing can be seen in Fig. 2(a), up to 73% for sample AA 3ML and up to 60% for sample AA 6ML. Annealing of samples BA 3ML results in concentric core/shell QDs and produces an alloyed interface, which reduces not only the lattice strain but probably the number of defects at the CdSe/CdS interface [13], which is beneficial for reaching high PL QY values. A strong confinement of the hole within the core and

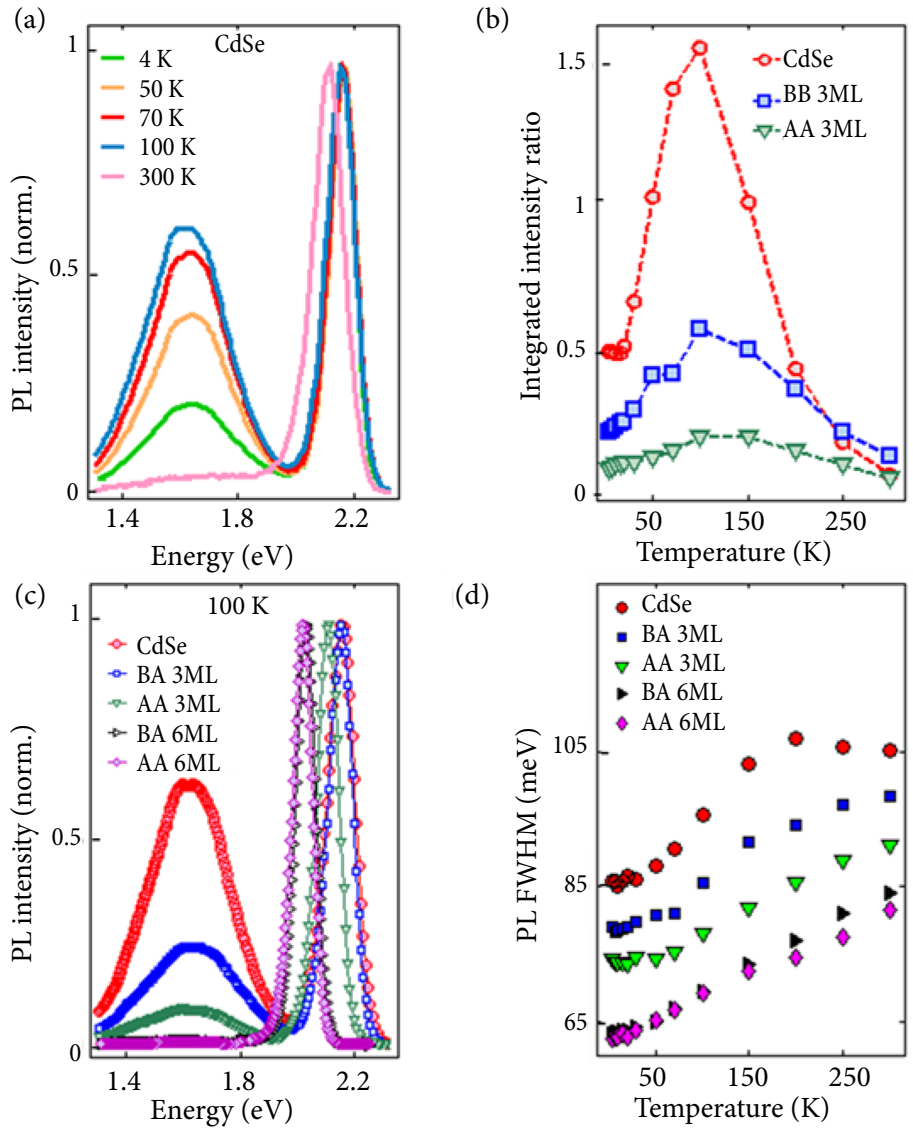

Fig. 3. Representative temperature-dependence of (a) the normalized PL spectra of CdSe core QDs recorded at various temperatures from 4 to 300 K. The temperature is given in the legend. The intensity of the PL spectra at various temperatures is normalized relative to the dominant exciton PL band intensity at 300 K. (b) Ratio of the integrated PL intensities of the surface trap band to their corresponding excitonic PL band of CdSe core QDs and CdSe/CdS core/shell samples, as listed in the legend. (c) Effect of shell formation on the PL spectra of all investigated core/shell QDs at 100 K, as given in the legend. The intensity of the PL spectra is normalized to the dominant exciton PL band edge intensity of CdSe core QDs. (d) Temperature-dependence of the dominant exciton PL FWHM of the samples as given in the legend. The QDs dispersed in epoxy resin.

delocalization of the electron throughout the entire CdSe/CdS core/shell QD is indicative of a quasi-type-II structure [8, 20, 32] which explains the size-dependent red-shift of the E_g observed above.

Thermally activated processes in the QDs were studied by following the variation in the absorption and emission spectra as a function of temperature. Figure 2(b) illustrates a representative set of the absorption and cw-PL spectra of the BA 6ML sample, recorded at various temperatures from 4 to 300 K; the samples were dispersed in epoxy resin and kept under oxygen-free conditions. The absorption and cw-PL spectra are dominated by excitonic transitions with energy $E_{1Sh3/2-1Se1/2}$ and are blue-shifted with the decrease in temperature, resembling a trend found in high energy band gap II–VI semiconductors.

Temperature-dependent PL measurements of the CdSe core and corresponding CdSe/CdS core/shell QDs can provide information related to the suppression of the trap-surface emission band and electron-phonon interactions. Figure 3(a) shows the temperature-dependent PL spectra (normalized to the exciton emission band) of CdSe core QDs, which at RT consist only of the near-band gap emission (E_{PL}) band centered at about 2.2 eV. In contrast, at low temperatures, the PL spectrum contains an additional broad deep emission band with the full width at half maximum (FWHM) = 400 meV centered around 1.6 eV, significantly red-shifted from the QDs E_g and caused by surface-state-mediated recombination [33, 34]. Figure 3(b) illustrates the temperature-dependent evolution of the surface trap band integrated PL intensities of CdSe core, BA 3ML and AA 3ML samples, relative to their corresponding normalized excitonic emission band integrated intensity. The integrated intensity of the trap-surface emission band for the core

and 3ML QDs samples reaches its peak value at temperature T = 100 K. The effect of shell formation on the PL spectra of the investigated core/shell QDs at 100 K is illustrated in Fig. 3(c), the spectra are normalized to the exciton emission PL band intensity. The results reveal the following: (1) suppression (up to 50%) of the trap emission band intensity during shell growth in 3ML samples; (2) further remarkable suppression of the trap band is achieved (up to 90%) by the annealing process of the sample. As this takes place, the exciton emission band FWHM, as seen in Fig. 3(c), becomes even narrower. In samples with a 6ML shell, the trap emission band is completely suppressed.

Figure 3(d) represents the FWHM of the dominant exciton PL band as a function of temperature for the samples investigated, revealing a continuous line broadening with the increase in temperature. The FWHM of the exciton PL bands are characterized by an inhomogeneous, temperature independent broadening and a homogeneous broadening that derives from temperature dependent exciton–phonon interactions. The inhomogeneous broadening parameter (Γ_{inh}) can be defined at low (4 K) temperature and depends on the size, shape and shell inhomogeneity within the QDs ensemble. The figure shows that Γ_{inh} values obtained at 4 K decrease with the increase of shell thickness from 88 meV for CdSe core QDs to 80 meV for 3ML samples, and 63 meV for 6ML core/shell QDs. The Γ_{inh} decreasing upon the growth of the shell thickness revealed that the size distribution of the core/shell QDs was nearly nondispersive. It is seen in the figure that Γ_{inh} values in 3ML samples further decrease after annealing, down to 75 meV, confirming improved shell homogeneity of the core/shell structure due to the formation of a thin alloyed interface layer with the pronounced suppression of the defects number at the CdSe/CdS interface. Only a negligible decrease in Γ_{inh} values was observed after annealing in 6ML core/shell QDs revealing the absence of any change in the core/shell structure.

Figure 4(a) presents the E_g values as a function of T for the investigated samples. The figure reveals that E_g is red-shifted with the increase in temperature for both core and core/shell samples, which can be explained by the lattice deformation potential and exciton–phonon coupling typical to the wide band gap II–VI semiconductors [35]. Up to about 30 K, E_g has only slight temperature dependence, while at higher temperatures >30 K it decreases steadily. Furthermore, as seen in Fig. 4(a), the E_g values in core/shell samples with various shell thickness present different temperature dependence rates, e. g. a smaller band-edge temperature coefficient in core/shell QDs with respect to the primary cores, suggesting thermal stability. Annealing of the core/shell samples has no additional influence on the E_g rate of decrease.

Figure 4(b) illustrates the temperature dependence of the emission Stokes shift energy (E_S) calculated from the difference between E_g and E_{PL} values of the listed samples, and shows a decrease of the E_s with temperature growth. The E_s curve of the CdSe core shows the temperature dependence similar to that described in Ref. [36], and can be characterized by size, exciton fine structure, exciton–phonon coupling, PL inhomogeneous and homogeneous broadening. The curves in Fig. 4(b) show that the values of E_S in core/shell QDs decrease with the increase in shell thickness and temperature which may be related to the following factors: (1) an increase of the overall QDs size due to shell width growth, (2) variation of the exciton fine structure and exciton–phonon interaction due to a quasi-type-II band alignment, with respect to pure CdSe core QDs. The annealed core/shell QDs do not show any change in E_S temperature dependence with comparison to the only coated core/shell QDs, revealing that E_s at T = constant is determined only by shell thickness.

4. Conclusions

In summary, the studies of the temperature dependent absorbance and PL properties of CdSe/CdS core/shell

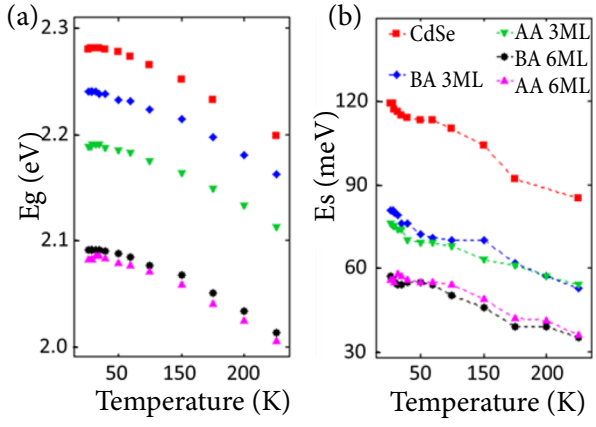

Fig. 4. Representative temperature-dependence of: (a) band gap energy (E_g) of CdSe core (red online) with r = 1.7 ± 0.5 nm and the corresponding CdSe/CdS QDs after coating at 100 °C (blue and black online, BA3 ML and BA6 ML), and after annealing at 130 °C (green and magenta online, AA 3ML and AA 6ML) as shown in the legends of (b); (b) Stokes shift energy (E_S) of the QD samples as listed in the legend, embedded in epoxy resin matrix.

samples with 3ML and 6ML shells after CdS coating on the CdSe core at 100 °C and followed by annealing at 130 °C led us to conclude the following: (1) low temperature coating forms 3ML core/shell QDs with inhomogeneous shell thickness; (2) coating of 6ML forms homogenous shell thickness; (3) the shell coating process is accompanied, in both 3ML and 6ML samples, with suppression of the number of defects at the CdSe core surface revealing enhanced PL QY.

Analysis of the spectroscopic results suggests that the CdS coating on the CdSe core at low temperature induces lattice strain in the core/shell structure, while PL QY was enhanced remarkably. The annealing that followed significantly improved the shell homogeneity of the 3ML QDs sample due to the formation of a thin alloyed interface with the pronounced suppression of the number of defects at the CdSe/CdS interface, gave rise to an E_g red-shift and a reducing PL inhomogeneous broadening parameter obtained at 4 K. This reveals the transformation of the core/shell QDs structure from a nonconcentric with inhomogeneous shell thickness to a concentric with homogeneous shell thickness structure. In contrast, the annealing of the 6ML core/shell structure causes only a small change in PL QY, due to the already concentric core/shell structure before annealing. This study provides sufficient evidence that it is possible to grow CdSe/CdS core/shell heterostructures with high PL QY and high photostability using low temperature preparation processes.

Acknowledgements

The authors acknowledge support of the Israel Council for High Education – Focal Area Technology (No. 872967), the Volkswagen Stiftung (No. 88116), and the Niedersachsen-Deutsche Technion Gesellschaft E. V. (No. ZN2916)

References

[1] A.H. Mueller, M.A. Petruska, M. Achermann, D.J. Werder, E.A. Akhadov, D.D. Koleske, M.A. Hoffbauer, and V.I. Klimov, Multicolor light-emitting diodes based on semiconductor nanocrystals encapsulated in GaN charge injection layers, Nano Lett. **5**, 1039–1044 (2005).

[2] M.J. Bowers, J.R. McBride, and S.J. Rosenthal, White-light emission from magic-sized cadmium selenide nanocrystals, J. Am. Chem. Soc. **127**, 15378–15379 (2005).

[3] L.G. Wang, S.J. Pennycook, and S.T. Pantelides, The role of the nanoscale in surface reactions: CO_2 on CdSe, Phys. Rev. Lett. **89**, 075506 (2002).

[4] J.P. Zimmer, S. Kim, S. Ohnishi, E. Tanaka, J.V. Frangioni, and M.G. Bawendi, Size series of small indium arsenide–zinc selenide core–shell nanocrystals and their application to *in vivo* imaging, J. Am. Chem. Soc. **128**, 2526–2527 (2006).

[5] D.L. Klein, R. Roth, A.K.L. Lim, A.P. Alivisatos, and P.L. McEuen, A single-electron transistor made from a cadmium selenide nanocrystal, Nature **389**, 699–701 (1997).

[6] X.Y. Wang, L.H. Qu, J.Y. Zhang, X.G. Peng, and M. Xiao, Surface-related emission in highly luminescent CdSe quantum dots, Nano Lett. **3**, 1103–1106 (2003).

[7] J.J. Li, Y.A. Wang, W. Guo, J.C. Keay, T.D. Mishima, M.B. Johnson, and X. Peng, Large-scale synthesis of nearly monodisperse CdSe/CdS core/shell nanocrystals using air-stable reagents via successive ion layer adsorption and reaction, J. Am. Chem. Soc. **125**, 12567–12575 (2003).

[8] X. Peng, M.C. Schlamp, A.V. Kadavanich, and A.P. Alivisatos, Epitaxial growth of highly luminescent CdSe/CdS core/shell nanocrystals with photostability and electronic accessibility, J. Am. Chem. Soc. **119**, 7019–7029 (1997).

[9] I. Mekis, D.V. Talapin, A. Kornowski, M. Haase, and H. Weller, One-pot synthesis of highly luminescent CdSe/CdS core/shell nanocrystals via organometallic and "greener" chemical approaches, J. Phys. Chem. B **107**, 7454–7462 (2003).

[10] U. Banin, M. Bruchez, A.P. Alivisatos, T. Ha, S. Weiss, and D.S. Chemla, Evidence for a thermal contribution to emission intermittency in single CdSe/CdS core/shell nanocrystals, J. Chem. Phys. **110**, 1195–1201 (1999).

[11] B.O. Dabbousi, J. Rodriguez-Viejo, F.V. Mikulec, J.R. Heine, H. Mattoussi, R. Ober, K.F. Jensen, and M.G. Bawendi, (CdSe)ZnS core–shell quantum dots: synthesis and characterization of a size series of highly luminescent nanocrystallites, J. Phys. Chem. B **101**, 9463–9475 (1997).

[12] M.A. Hines and P. Guyot-Sionnest, Synthesis and characterization of strongly luminescing ZnS-capped CdSe nanocrystals, J. Phys. Chem. **100**, 468–471 (1996).

[13] R.G. Xie, U. Kolb, J.X. Li, T. Basche, and A. Mews, Synthesis and characterization of highly luminescent CdSe-core CdS/$Zn_{0.5}Cd_{0.5}$S/ZnS multishell nanocrystals, J. Am. Chem. Soc. **127**, 7480–7488 (2005).

[14] C.B. Murray, D.J. Norris, and M.G. Bawendi, Synthesis and characterization of nearly monodisperse CdE (E = sulfur, selenium, tellurium) semiconductor nanocrystallites, J. Am. Chem. Soc. **115**, 8706–8715 (1993).

[15] D.V. Talapin, A.L. Rogach, A. Kornowski, M. Haase, and H. Weller, Highly luminescent monodisperse CdSe and CdSe/ZnS nanocrystals synthesized

in a hexadecylamine–trioctylphosphine oxide–trioctylphospine mixture, Nano Lett. **1**, 207–211 (2001).

[16] X. Peng, L. Manna, W. Yang, J. Wickham, E. Scher, A. Kadavanich, and A.P. Alivisatos, Shape control of CdSe nanocrystals, Nature **404**, 59–61 (2000).

[17] K. Boldt, N. Kirkwood, G.A. Beane, and P. Mulvaney, Synthesis of highly luminescent and photo-stable, graded shell CdSe/$Cd_xZn_{1-x}S$ nanoparticles by *in situ* alloying, Chem. Mater. **25**, 4731–4738 (2013).

[18] O. Chen, J. Zhao, V.P. Chauhan, J. Cui, C. Wong, D.K. Harris, H. Wei, H. Han, D. Fukumura, R.K. Jain, and M.G. Bawendi, Compact high-quality CdSe-CdS core–shell nanocrystals with narrow emission linewidths and suppressed blinking, Nat. Mater. **12**, 445–451 (2013).

[19] N. Tschirner, H. Lange, A. Schliwa, A. Biermann, C. Thomsen, K. Lambert, R. Gomes, and Z. Hens, Interfacial alloying in CdSe/CdS heteronanocrystals: a Raman spectroscopy analysis, Chem. Mater. **24**, 311–318 (2011).

[20] W.K. Bae, L.A. Padilha, Y. Park, H. McDaniel, I. Robel, J.M. Pietryga, and V.I. Klimov, Controlled alloying of the core–shell interface in CdSe/CdS quantum dots for suppression of auger recombination, ACS Nano **7**, 3411–3419 (2013).

[21] F. Todescato, A. Minotto, R. Signorini, J.J. Jasieniak, and R. Bozio, Investigation into the heterostructure interface of CdSe-based core–shell quantum dots using surface-enhanced Raman spectroscopy, ACS Nano **7**, 6649–6657 (2013).

[22] G.E. Cragg and A.L. Efros, Suppression of Auger processes in confined structures, Nano Lett. **10**, 313–317 (2010).

[23] R. Vaxenburg and E. Lifshitz, Alloy and heterostructure architectures as promising tools for controlling electronic properties of semiconductor quantum dots, Phys. Rev. B **85**, 075304 (2012).

[24] J.I. Climente, J.L. Movilla, and J. Planelles, Auger recombination suppression in nanocrystals with asymmetric electron–hole confinement, Small **8**, 754–759 (2012).

[25] W. Nan, Y. Niu, H. Qin, F. Cui, Y. Yang, R. Lai, W. Lin, and X. Peng, Crystal structure control of zinc-blende CdSe/CdS core/shell nanocrystals: synthesis and structure-dependent optical properties, J. Am. Chem. Soc., **134**(48), 19685 (2012).

[26] N. Grumbach, R.K. Capek, E. Tilchin, A. Rubin-Brusilovski, J. Yang, Y. Ein-Eli, and E. Lifshitz, Comprehensive route to the formation of alloy interface in core/shell colloidal quantum dots, J. Phys. Chem. C **119**, 12749–12756 (2015).

[27] V.M. Dzhagan, M.Y. Valakh, A.E. Raevskaya, A.L. Stroyuk, S.Y. Kuchmiy, and D.R.T. Zahn, Resonant Raman scattering study of CdSe nanocrystals passivated with CdS and ZnS, Nanotechnology **18**, 285701 (2007).

[28] V.M. Dzhagan, M.Y. Valakh, A.G. Milekhin, N.A. Yeryukov, D.R.T. Zahn, E. Cassette, T. Pons, and B. Dubertret, Raman- and IR-active phonons in CdSe/CdS core/shell nanocrystals in the presence of interface alloying and strain, J. Phys. Chem. C **117**, 18225–18233 (2013).

[29] K. Gong and D.F. Kelley, Lattice strain limit for uniform shell deposition in zincblende CdSe/CdS quantum dots, J. Phys. Chem. Lett. **6**, 1559–1562 (2015).

[30] G. Zaiats, A. Shapiro, D. Yanover, Y. Kauffmann, A. Sashchiuk, and E. Lifshitz, Optical and electronic properties of nonconcentric PbSe/CdSe colloidal quantum dots, J. Phys. Chem. Lett. **6**, 2444–2448 (2015).

[31] A. Minotto, F. Todescato, I. Fortunati, R. Signorini, J.J. Jasieniak, and R. Bozio, Role of core–shell interfaces on exciton recombination in CdSe–$Cd_xZn_{1-x}S$ quantum dots, J. Phys. Chem. C **118**, 24117–24126 (2014).

[32] F. Garcia-Santamaria, S. Brovelli, R. Viswanatha, J.A. Hollingsworth, H. Htoon, S.A. Crooker, and V.I. Klimov, Breakdown of volume scaling in Auger recombination in CdSe/CdS heteronanocrystals: the role of the core–shell interface, Nano Lett. **11**, 687–693 (2011).

[33] J. Mooney, M.M. Krause, J.I. Saari, and P. Kambhampati, Challenge to the deep-trap model of the surface in semiconductor nanocrystals, Phys. Rev. B **87**, 081201(R) (2013).

[34] M.M. Krause, J. Mooney, and P. Kambhampati, Chemical and thermodynamic control of the surface of semiconductor nanocrystals for designer white light emitters, ACS Nano **7**, 5922–5929 (2013).

[35] M.R. Salvador, M.W. Graham, and G.D. Scholes, Exciton–phonon coupling and disorder in the excited states of CdSe colloidal quantum dots, J. Chem. Phys. **125**, 184709 (2006).

[36] T.J. Liptay, L.F. Marshall, P.S. Rao, R.J. Ram, and M.G. Bawendi, Anomalous stokes shift in CdSe nanocrystals, Phys. Rev. B **76**, 155314 (2007).

ŽEMOJE TEMPERATŪROJE VYKDOMO PADENGIMO IR GRŪDINIMO ĮTAKA CdSe/CdS BRANDUOLIO / APVALKALO KVANTINIŲ TAŠKŲ STRUKTŪRINĖMS IR OPTINĖMS SAVYBĖMS

M. Isarov, N. Grumbach, G.I. Maikov, J. Tilchin, Y. Jang, A. Sashchiuk, E. Lifshitz

Izraelio Techniono technologijos institutas, Haifa, Izraelis